ACS Sustainable Chemistry & Engineering

pubs.acs.org/journal/ascecg

Open Access

This article is licensed under CC-BY 4.0

Research Article

Physicochemical Insights into Enzymatic Polymerization of Lignosulfonates

Sebastian A. Mayr, Stefan Wagner, Roland Nagl, Alessandro Pellis, Matteo Gigli, Claudia Crestini, Melissa Horvat, Tim Zeiner, Georg M. Guebitz, Renate Weiss,* and Nikolaus Schwaiger

Cite This: https://doi.org/10.1021/acssuschemeng.3c05521

Read Online

ACCESS | Metrics & More | Article Recommendations | Supporting Information

ABSTRACT: The enzyme-catalyzed polymerization of lignosulfonates was investigated. Molecular formulas for the initial material (LS) and the final polymerized lignosulfonates (pLS) were determined by mass balance calculations combined with elemental analyses, allowing the elaboration of the reaction equation. Structural and chemical changes during the reaction were followed. Rheology and size exclusion chromatography showed that viscosity and molecular weight increased 90-fold and 4-fold, respectively. The thermal stability of pLS was investigated by thermogravimetric analysis and was found to be rather low compared to those of other polymers. The specific heat capacity (c_p) was determined by differential scanning calorimetry and was higher for pLS than for LS, depending on the final formulation of the polymer. Determination of the higher heating value together with the reaction equation allowed the determination of the reaction enthalpy of −61 kJ/kg_{feed}. Only minor structural changes were revealed by NMR and FTIR analyses. However, these are responsible for the gained insolubility properties of pLS. Higher solubility in organic solvents of varying polarity (heptane, toluene, isopropanol, and acetone) was found for polymer films. The perturbed chain statistical associating fluid theory equation of state was found suitable to model the solution behavior of pLS films.

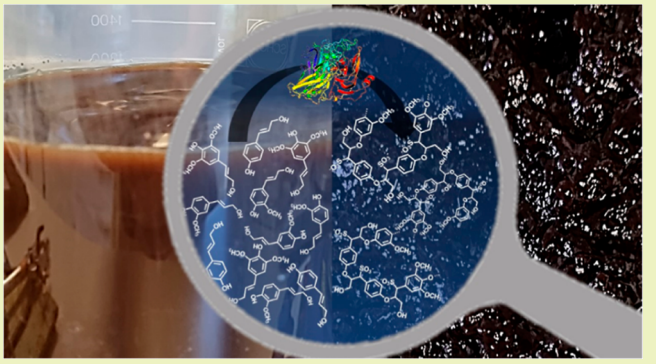

KEYWORDS: *biorefinery, enthalpy, laccase, mass balance, fluid theory*

Downloaded via UNIV BODENKULTUR WIEN on November 29, 2023 at 07:32:32 (UTC).
See https://pubs.acs.org/sharingguidelines for options on how to legitimately share published articles.

1. INTRODUCTION

Accumulation of waste in landfills and climate change are two of the major problems faced by today's society. Huge efforts are currently being made to develop novel processes to reduce greenhouse gas emissions and waste generation. Possible ways to achieve these goals are the improvement of recycling rates, the intensified use of recycled materials in new products, and the replacement of petroleum-based materials with biobased ones. At the same time, steps toward the reduction of waste generation should be taken. The implementation of circular bioeconomy pathways aims at solving this issue by exploiting renewable and thus CO_2-neutral resources to generate high-added value products. Additionally, the generated waste streams shall be reprocessed and/or upcycled into valuable products. Finally, after severe lifetime extension and reuse, the chemically bonded energy may be used for power generation and shall fuel further processes.[1,2]

In biorefinery applications, lignocellulosic biomass, composed of cellulose, hemicellulose, and lignin, is adopted as the starting material. Specifically, lignin is a complex, recalcitrant, and heterogeneous material consisting of polyaromatic compounds. For all these reasons, its application in commodities is highly challenging.[3−5] Lignins from different origins are based on three repetitive phenylpropanoid units, the so-called monolignols, namely, *p*-hydroxyphenyl (H), guaiacyl (G), and syringyl (S), differing only in the number of methoxy groups attached to the aromatic ring. The H-unit does not have any methoxy groups, G has one at position C3 and S has two at positions C3 and C5. These monolignols can form a variety of different interunit linkages (reactive alkyl or aryl ether or ester bonds but also unreactive carbon−carbon bonds). The possible linkages are defined by the distribution of the monolignols, which vary in the different kinds of biomass (hardwood, softwood, or herbaceous). Softwoods are mainly composed of G-units (forming branched polymers), hardwoods contain both G- and S-units (leading to mainly linear polymers) with minor amounts of H-units for both, while herbaceous biomass, such as grasses, consists of H-, G-, and S-units.[6] Despite its complexity and recalcitrance, nature found

Received: August 30, 2023
Revised: November 17, 2023
Accepted: November 17, 2023

© XXXX The Authors. Published by American Chemical Society

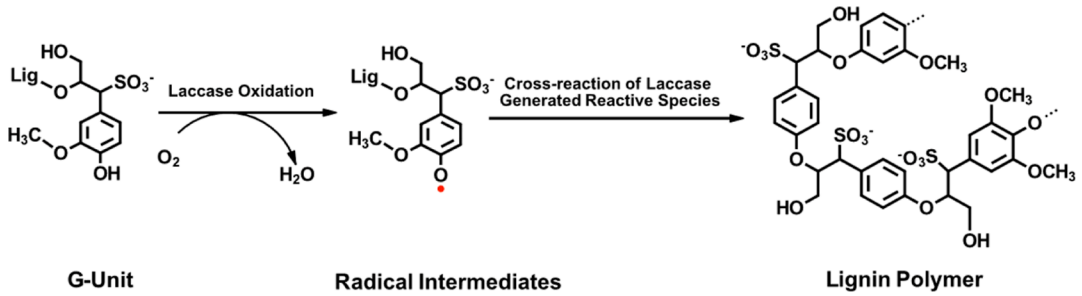

Figure 1. Laccase-mediated oxidation of LS to pLS (adapted from Mayr et al. 2021). Show exemplarily for the lignin G-unit (the main monolignol unit in softwood). Oxidation of LS by laccase leads to the formation of radical intermediates, which can react further, while simultaneously molecular oxygen is reduced to water.

ways to degrade lignin by evolving a consortium of different enzymes capable of breaking down the lignin polymer into smaller compounds. One of these enzyme groups is represented by laccases (EC 1.10.3.2). They are copper-containing oxidoreductases able to oxidize mainly phenolic residues that are present, e.g., in lignin, to radicals by simultaneously reducing molecular oxygen to water. The generated phenoxyl radicals can further react with each other leading to the formation of bigger lignin polymers (Figure 1).[7−10] This reaction mechanism provides laccases with the ability to synthesize or degrade lignin. Plant laccases primarily synthesize lignin, while those of fungal or bacterial origin are mainly responsible for lignin degradation.[7,8,11] The direction of laccase activity can be determined by the reaction conditions. However, the parameters for the reaction depend on both the laccase as well as the substrate.[12] Thus, a process using the water-soluble lignosulfonate (LS) in combination with a laccase isolated from the fungus *Myceliophthora thermophila* (MtL)[13] requiring only water and oxygen at moderate temperatures and neutral pH, without the need for expansive and sometimes toxic mediators, was developed to achieve extensive polymerization of LS by setting the reaction conditions accordingly. This process was found to lead to water insolubility of LS, increase dispersibility, and generate water as the only byproduct.[14,15] All the different process parameters have been investigated and optimized: (i) the reaction conditions necessary to get highly polymerized LS in a reasonable time,[16] (ii) the use of different enzymes,[17] (iii) the effect of different downstream methods on the reactivity of LS,[18] and (iv) the suitability of other technical lignins.[19,20] On these bases, a variety of applications, such as hydrogels, coatings, or adhesives,[21−26] are already well implemented. Further, new possibilities to extend the application range, such as enzymatic coupling of foreign molecules onto LS to tailor its properties, are under investigation.[9] As can be seen, although this enzymatic polymerization process of LS is well characterized and implemented now, the underlying reaction mechanisms are still not completely understood. Knowledge of these mechanisms will help in unraveling the reaction stoichiometry and thermodynamic parameters of the reaction, allowing further knowledge-based exploitation of this process.

This study aims at characterizing the structural changes that occur during enzymatic polymerization of LS under the conditions optimized in previous studies,[15−20] thereby unraveling the reaction stoichiometry and the thermodynamic parameters. This allowed for the first time the establishment of a reaction equation of the enzymatic LS polymerization reaction and further determination of the enthalpy of the reaction. Finally, the resulting polymers were investigated for their solubility in different organic solvents of varying polarity. The results were then used to test the reliability of a prediction model of polymer solubility using the perturbed chain statistical associating fluid theory (PC-SAFT) method.

2. MATERIALS AND METHODS

2.1. Materials. All used chemicals were purchased from Sigma-Aldrich (Steinheim, Germany) or Merck (Darmstadt, Germany) and were of analytical grade, while *M. thermophila* laccase (MtL) was from Novozymes (Novozyme 51003, Bagsveard, Denmark). The softwood magnesium lignosulfonate used originates from spent liquor generated during the sulfite wood pulping process and was kindly provided by Sappi Paper Holding GmbH.

2.2. Laccase Activity Assay. Laccase activity was assayed by monitoring the oxidation of 2,2′-azino-bis(3-ethylbenzothiazoline-6-sulfonic acid) diammonium salt (ABTS) to its cation radical. The resulting reaction product was quantified at 420 nm by using a plate reader (Tecan, Infinite M200, Switzerland). For the reaction, 170 μL of the enzyme diluted in 0.1 M sodium phosphate buffer (pH 7) was mixed with 50 μL of a 0.1 M ABTS solution. The activity was expressed in nanoKatal/mL (nKat/mL) and transformed into units/mL (U/mL) by multiplying the value by 16.67 (one unit is defined as the amount of enzyme necessary to convert 1 μmol of substrate per minute). All samples were measured in triplicate.

2.3. Enzymatic Oxidation of Lignosulfonate. Laccase-catalyzed polymerization was carried out in four 1 L glass reaction vessels containing 500 mL of a 21% (w/v) LS solution adjusted to pH 7 using 5 M NaOH, at 22.6 °C and an oxygen flow rate equal to 52 mL/min. The reaction was started by adding 10 U/mL MtL. Water from the exhaust gas was condensed in a cool trap. The final gel-like products from the four reaction vessels were mixed and partially poured into films, while the other part was dried (either through lyophilization or at room temperature) in the form of granulates for further analyses. (An overview of the reaction conditions and setup is given in the Supporting Information; Table S1 and Figure S1).

2.4. Fourier Transform Infrared Spectroscopy. The powdered samples were analyzed by Fourier transform infrared spectroscopy (Bruker Vortex 70, Bruker Corporation, Billerica, MA, USA) operated in the ATR mode. The spectra were recorded in the range from 4000 to 400 cm^{-1} with a resolution of 2 cm^{-1} and a total number of 128 scans in drift mode.

2.5. Viscosity Measurement. Viscosity was followed during the incubation period as a fast, indirect way to determine the increase in molecular weight and to set the end point of the reaction. For the measurement, 700 μL of the sample was applied to the Rheometer (MCR 302, Anton Paar, Austria) equipped with a measuring system consisting of a cone plate with a diameter of 50 mm and an angle of 1° (CP50-1). The viscosity measurement was done for 10 s with measuring points made every second at a constant temperature of 20 °C and a constant shear rate of 200 s^{-1}. Data analyses were performed with Anton Paar software RheoCompass 1.24. All samples were measured in duplicate.

https://doi.org/10.1021/acssuschemeng.3c05521
ACS Sustainable Chem. Eng. XXXX, XXX, XXX−XXX

2.6. Size Exclusion Chromatography Coupled to a Multi-angle Laser Light Scattering Detector. The molecular weights of the samples were determined by using size exclusion chromatography (SEC). A liquid chromatography system equipped with a quaternary/binary pump, autosampler 1260 series, a diode array detector (DAD), a refractive index (RI) detector system (Agilent Technologies 1260 Infinity), and a MALLS HELEOS DAWN II detector (Wyatt Technology, Santa Barbara, CA, USA) was used. The columns used consisted of a precolumn PL aqua gel−OH MIXED guard (PL1149-1840, 8 μm, 7.5 × 50 mm^2, Agilent, Palo Alto, CA) and a separation column PL aqua gel−OH MIXED H (PL1549-5800, 8 μm, 4.6 × 250 mm^2, Agilent, Palo Alto, CA) with a range from 6 to 10,000 kDa. The mobile phase contained 50 mM $NaNO_3$ with 200 mg/L NaN_3. The sample injection volume was 100 μL, and the total runtime for one sample was 90 min. The samples were diluted with the mobile phase to a concentration of 1 mg/mL and filtered through a 0.45 μm syringe filter before being loaded onto the column. The internal system calibration of the detector is controlled with BSA and dextran standards from 6 to 600 kDa. For normalization, band broadening, and alignment of the MALLS detector, a BSA standard was used. The software used for data acquisition and analysis was ASTRA 7 software from Wyatt Technologies.

2.7. Field Flow Fractionation Coupled to a MALLS Detector. The molecular weight distribution of the samples was additionally determined by using the Wyatt Eclipse NEON field flow fractionation system (Wyatt Technology, Santa Barbara, CA, USA). The chromatography system was equipped with a quaternary/binary pump, autosampler 1260 series, a diode array detector (DAD), a RI detector system (Agilent Technologies 1260 Infinity), and a MALLS HELEOS DAWN II detector (Wyatt Technology, Santa Barbara, CA, USA) was used. The field flow fractionation was run with the Eclipse long channel with a spacer height of 350 μm and a 10 kDa cellulose membrane. The mobile phase contained 50 mM $NaNO_3$ with 200 mg/L NaN_3. The sample injection volume was 50 μL, and the total runtime for one sample was 80 min. The samples were diluted with the mobile phase to a concentration of 2 mg/mL. The internal system calibration of the detector is controlled with BSA and dextran standards from 6 to 600 kDa. For normalization, band broadening, and alignment of the MALLS detector, a BSA standard was used. The software used for data acquisition and analysis was ASTRA 8.2 software from Wyatt Technologies.

2.8. Heteronuclear Single Quantum Coherence Nuclear Magnetic Resonance Spectroscopy. The measurements were carried out on a 400 MHz Bruker NMR spectrometer (Bruker Corporation, Billerica, MA, USA). One hundred (100) mg of LS sample was dissolved in 600 μL of DMSO-d_6. The measurements were performed as previously reported.[27]

2.9. High-Performance Liquid Chromatography. For high-performance liquid chromatography (HPLC) measurements an Agilent 1260 LC system (Agilent Technologies, Santa Clara, USA), with an ion exchange column ION-300 (Transgenomic Inc.) was used. The eluent used was 0.01 N H_2SO_4 with a flow rate of 0.3 mL min^{-1} at a constant temperature of 45 °C. The injection volume of the sample was 40 μL with a runtime of 120 min. Detection of the released products was measured with a RID detector. For calibration, the respective standards were measured over a concentration range from 1 to 1000 mg/L.

2.10. Gas-Phase Chromatography Mass Spectrometry. Condensed water from the exhaust gas was analyzed for organic constituents by gas chromatography (GC) using a Shimadzu GC 2010 coupled with a Shimadzu GCMS QP 2010 Plus quadrupole mass spectrometer. The GC was equipped with an Agilent VF-1701 MS column (60 m × 0.25 mm × 0.25 μm) and a Shimadzu AOC-5000 autosampler. The sample injection volume was 5 μL with a 1:30 split ratio, and a temperature program with heating from 40 to 280 °C over 5 min, followed by a plateau time at 280 °C of 10 min, was applied.

2.11. Solvent Uptake and Solubility of the Lignosulfonate Polymer. To determine the solvent uptake, the final reaction product in both film and granule form was immersed in organic solvents of different polarities (heptane, isopropanol, acetone, and toluene). Samples were air-dried before the solvent uptake experiments until their mass no longer decreased. Subsequently, the samples were submersed in the solvents, and the respective solvent uptake was determined gravimetrically for 6 weeks in regular intervals. The solvent uptake is calculated as the mass increase in relation to the air-dried sample mass in milligrams of solvent uptake per gram of dry sample, which can be converted to mass-% related solvent uptake by multiplying by a factor of 10. Solvent weight fractions in polymer samples after equilibrium solvent uptake were determined by the evaporation of the solvent. For that purpose, polymer samples were dried at T = 100 °C at ambient pressure for 1 week. Weight loss due to solvent evaporation was then determined gravimetrically by comparing sample weights before and after drying. All weight measurements were performed on a Sartorius Secura 26-1CEU microbalance with a linearity error of 0.01 mg.

2.12. Differential Scanning Calorimetry. Differential scanning calorimetry was conducted in the temperature range from 25 to 180 °C with a heating rate of 10 °C/min. A Linseis Chip-DSC 10 device (Linseis GmbH, Selb, Germany) was used and placed in a temperature-controlled chamber to ensure constant ambient conditions. The specific heat capacity c_p was determined using the sapphire method for calibration; the melting point and enthalpy of fusion of indium, zinc, and tin were measured.

2.13. Thermogravimetric Analyses. The measurements were carried out under a nitrogen atmosphere with a flow rate of 20 mL/min on a PerkinElmer TGA 4000 device (PerkinElmer, Waltham, MA, USA). The temperature range was from 50 to 900 °C with a heating rate of 10 °C/min.

2.14. Elemental Analysis. The measurements were conducted with a Thermo Scientific Flash Smart CHNS. Accurately weighted and dried samples (2−3 mg) were placed on a tin foil with 10 mg of V_2O_5 to be folded and tightly pressed before analysis. Each sample was measured 4 times. The deviation is between 0.30% (C), 0.17% (H), and 0.27% (S), slightly depending on the element.

2.14.1. Ash Determination. Samples were dried at 105 °C for 24 h and subsequently incinerated at 800 °C. Ash was determined once, standard deviation was determined with <0.08%.

2.15. Determination of Heating Value. Bone dry samples were pelletized and incinerated in an oxygen atmosphere according to DIN 51900 and DIN EN ISO 18125 with an IKA C6000 global standards calorimeter. Samples were determined 6 times. The standard deviation is below 1.5%.

2.16. Perturbed Chain Statistical Associating Fluid Theory. The solvent uptake and the density of the LS polymer were modeled with the perturbed chain statistical associating fluid theory (PC-SAFT)[28−30] equation of state. Since its development in 2001, PC-SAFT has been widely established as a suitable model for thermodynamic properties of polymer systems[30−34] and even biopolymers such as proteins[35,36] in the literature. PC-SAFT describes the Helmholtz free energy A of the polymer + solvent system based on a hard-chain reference fluid. The model considers ideal (A_{id}), hard-chain (A_{hc}), dispersive (A_{disp}), and associating (A_{assoc}) contributions between segments to the Helmholtz energy.

To account for the dipole moment of polar molecules such as acetone, the polar contribution to the Helmholtz energy A_{dipol} according to Gross and Vrabec[37] has further been included in the model framework (eq 1). A more detailed description of the model and its application to polymer phase equilibria is described in the literature by Krenn et al.[32]

$$A = A_{id} + A_{hc} + A_{disp} + A_{assoc} + A_{dipol} \quad (1)$$

The polymer density and equilibrium properties of mixtures with solvents can consequently be calculated from the compressibility factor $Z = P_v/RT$, whereby P is the system pressure, v is the molar volume, R is the universal gas constant, and T is the system temperature. Analogously to the Helmholtz free energy, Z can be calculated as the sum of individual contributions (eq 2) corresponding to the free energy contributions in eq 1.

https://doi.org/10.1021/acssuschemeng.3c05521
ACS Sustainable Chem. Eng. XXXX, XXX, XXX−XXX

$$Z=1+Z_{hc}+Z_{disp}+Z_{assoc}+Z_{elast}+Z_{dipol} \quad (2)$$

Notably, the elastic term, which is often used in literature to model the stretching of polymer chains,[32,38−40] is absent from eq 1. This approach has been chosen due to the comparatively low molecular weight of the produced pLS in contrast to cross-linked polymers such as epoxy resins or cross-linked PNIPAAm.[38] Moreover, the high solubility of pLS in isopropanol and acetone further suggests low cross-linking functionality and therefore low impact of the elastic forces within the pLS polymer on its thermodynamic properties.

3. RESULTS AND DISCUSSION

3.1. Mass Balance and Determination of the Reaction Equation. At first, the mass balance for the reaction was elaborated (Table 1). To this end, the weights of the reaction vessels were gravimetrically determined before and after the reaction, with an overall inaccuracy below 1% (a detailed list of the measurement is given in the Supporting Information; Tables S2 and S3). This enabled us to determine the overall mass as well as the solid and water contents before (LS) and after the reaction (pLS). The mass input was the amount of solid (LS), solvent (water), enzyme, and NaOH (for adjustment of the pH) added, while the mass output was the polymerized material. The overall mass was found to increase by 0.11% (Table 1). This confirms the reaction mechanism of laccase forming water with the supplied oxygen (Figure 1).[10,41] Due to the negative enthalpy of the formation of water (ΔH_f°) (Table 4),[42] this can be regarded as a first indication of an overall exothermic reaction. The dry substance was found to decrease by 1.10% (Table 1), which is a very low balance inaccuracy (detailed values for the determination of the dry substance are available in the Supporting Information Tables S4 and S5). To investigate this more closely, the exhaust gas was collected in a cooling trap, and the condensed water was analyzed for its carbohydrate and carboxylic acid content by HPLC and GC−MS. However, no traces of organic molecules were detected in the exhaust gas. This indicated that the stripping of smaller LS did not cause a difference in the solid content. However, laccase oxidation of LS causes abstraction of the hydrogen atoms of the phenolic residues which may be the reason for the determined decrease in solid content, since the hydrogen atoms react with oxygen to form water.[43] In the second step, a full elemental analysis was conducted (Table 2). The amounts of carbon ©, hydrogen (H), sulfur (S), nitrogen (N), and ash were measured, while oxygen content (O) was calculated by subtracting the sum of the determined elements from 100%. It is assumed that ash and nitrogen are not affected by laccase oxidation. Thus, they can be regarded as inert for this reaction and were neglected for further calculations. The elemental analyses revealed that carbon and sulfur contents were stable throughout the reaction. While a slight decrease in hydrogen content from 6.28 to 5.98% was observed, the oxygen content was found to increase from 30.59% at the beginning (LS) to 31.38% at the end (pLS) (Table 2). The uncertainties during the measurement were found to be only slightly above the background noise (see Materials and Methods section). The decrease in hydrogen content is related to phenoxyl radical formation, whereby the hydrogen atom is abstracted from the phenolic hydroxyl group. This would also explain the observed decrease in solid content as found before when the mass balance was set up (Table 1). The increase in oxygen content indicates incorporation of oxygen into LS, a mechanism also observed in oxidative processes such as delignification and ammonolysis, in which the oxygen pressure is a main driver of oxygen incorporation into technical lignins.[44,45] With the found elemental compositions, the molecular formulas of the compounds are $C_{23.16}H_{33.25}SO_{10.20}$ for LS and $C_{22.96}H_{31.40}SO_{10.38}$ for pLS. The formulas were calculated by multiplying the sample mass (LS and pLS, respectively) with their determined mass percent ratio, divided by the respective atomic weight and normalized to sulfur.[46] Thus, it can be concluded that these minor changes on the microscopic level induce outstanding macroscopic differences in the LS properties. With the gathered information, a reaction equation is accessible by support with a least-squares approximation (Reaction eq R1). The reaction equation shows that the hydrogen atoms of the phenolic hydroxyl groups were abstracted from the LS molecule due to oxidation by laccase, as can be seen in the decrease in the number of hydrogen atoms from 33.25 in each LS molecule (reactant on the left) to 31.40 in pLS (product on the right). Concomitantly, the number of oxygen atoms increased from 10.20 to 10.38 due to the incorporation of oxygen into LS, as

Table 1. Mass Balance for the Laccase Polymerization of the Initial Material (LS) to the Final Polymer (pLS)[a]

material	mass balance [g]	solid content [g]	water balance [g]
LS	1212.38	254.59	957.79
pLS	1213.66	251.78	961.88
deviation [g]	−1.28	2.81	−4.40
deviation [wt/wt]	−0.11%	1.10%	−0.46%

[a]The total, solid, and water mass were determined and balanced.

Table 3. Calorimetric Heating Values (HHV) Determined for LS and pLS after Laccase Polymerization

HHV	[kJ/kg]	[kJ/mol]
LS	−22.493	−11.412
pLS	−22.030	−11.142

Table 4. Data for the Standard Enthalpy of Formation (ΔH_f°)[a]

ΔH_f°	[kJ/mol]
LS	−2759
pLS	−2682
H_2O	−286
O_2	0

[a]The data for LS and pLS were determined, and those for H_2O and O_2 were taken from the literature.[50]

Table 2. Elemental Analysis and Ash Content on a Dry Basis for LS and pLS[a]

material	ash [wt/wt] (%)	C [wt/wt] (%)	H [wt/wt] (%)	N [wt/wt]	O [wt/wt] (%)	S [wt/wt] (%)
LS	4.74	52.14	6.28	<1	30.59	6.01
pLS	4.22	52.11	5.98	<1	31.38	6.06

[a]The values for ash, C, H, N, and S were determined, while the values for O were calculated.

https://doi.org/10.1021/acssuschemeng.3c05521
ACS Sustainable Chem. Eng. XXXX, XXX, XXX−XXX

Table 5. Viscosity, Molecular Weight (M_w and M_n), and Dispersity ($Đ$) Changes of LS, before (LS), and after (pLS) Laccase-Catalyzed Polymerization

	viscosity [mPa·s]	M_w [kDa]	M_n [kDa]	$Đ$ [M_w/M_n]
LS	7.06 ± 0.04	55.10 ± 0.39	32.98 ± 0.20	1.67 ± 0.02
pLS	638.25 ± 4.50	204.17 ± 5.35	68.93 ± 1.92	2.96 ± 0.01

also found by FTIR, shown further below. Generally, the reaction equation elucidates that only a few new chemical bonds are formed, while enzymatic oxidation is the dominant type of reaction, driven by the exothermic process of water formation.

Reaction equation 1: Laccase-catalyzed polymerization reaction of LS to pLS.

$$0.502C_{23.16}H_{33.25}SO_{10.20}+0.042O_2 \leftrightarrow 0.498C_{22.96}H_{31.40}SO_{10.38}+0.227H_2O$$

As expected from the elemental analyses, the reaction equation showed only minor changes in molecule composition, which confirms the results obtained so far.

3.2. Higher Heating Value and Enthalpy of Formation. Besides the stoichiometric description of a reaction in the form of a reaction equation, the thermochemical properties of a material are also of interest to gain a better understanding of the reaction. By knowing the enthalpy, one can predict whether a reaction releases (exothermic) or takes up (endothermic) energy. This is determined by incineration in a bomb calorimeter. With this method, it can be determined how much energy is stored in the material by measuring the amount of energy released by incineration in the presence of either oxygen or inert gases. Two types of heating values can be distinguished. The higher heating value (HHV) takes into account the heat of condensation of water, while the lower heating value (LHV) does not.[47] Herein, the HHV values for LS and pLS were determined by incineration with oxygen. It turned out that LS had a higher HHV than pLS (Table 3). This is in accordance with the higher oxygen content determined for pLS (Table 2) since the presence of oxygen leads to a lowering of the HHV.[48,49] These results confirm the findings made by elemental analyses (Table 2) and for the reaction equation (Reaction eq R1) presented before. Further, the lower HHV value of pLS again indicates nonenzymatic incorporation of small amounts of oxygen in addition to enzymatic polymerization.

According to Peduzzi et al.,[47] the standard enthalpy of formation (ΔH_f°) can be deduced from the incineration reaction with oxygen and the HHV. The HHV was determined by calorimetry (Table 3), while ΔH_f° data were taken from literature[50] (Table 4). Using Reaction R1 together with the data from Table 4 the enthalpy of the reaction (ΔH_R°) for the enzymatic LS polymerization can be determined. It is calculated by subtracting the sum of the enthalpies of the products from the sum of enthalpies of the reactants[51] and was found to be −60.84 kJ/kg_{feed} herein. This leads to a slightly exothermic reaction driven by water formation. This proves the observations made earlier when the mass balance.

3.3. Physicochemical Properties of LS Polymers. Upon laccase-catalyzed oxidation, the formed radicals can lead to the formation of quinone intermediates or productive coupling (β-O-4′, 4-O-5′, and C−C (5−5′) linkages) and thus polymerization, resulting in increased molecular weight and viscosity.[6,11,52,53] The viscosity increased 90-fold, from 7.06 to 638.25 mPa·s, leading to the formation of a gel-like material in the end. Determination of the molecular weight was done with an HPLC SEC-MALLS system, where the values of large fragments (mass average molecular weight; M_w) to the small fragments (number-average molecular weight; M_n) and their ratio (dispersity; $Đ$) can be determined. M_w was found to increase about 4-fold, from 55.10 to 204.17 kDa, while M_n and $Đ$ increased about 2-fold, from 32.98 to 68.93 kDa and from 1.67 to 2.69, respectively (Table 5). A detailed overview of the SEC-MALLS and viscosity determination is given in the Supporting Information Tables S6 and S7, and additionally the SEC-MALLS chromatograms of LS and pLS can be found there (Figure S2).

However, here it needs to be considered that the eluent used for the HPLC SEC-MALLS system was an aqueous one; thus, since the growing LS polymers become insoluble in water, the final polymers could not be fully dissolved anymore and only the remaining soluble fractions were analyzed. Additionally, previous attempts to dissolve the lignin polymers in organic solvents, such as DMSO, also failed. Therefore, a dissolution experiment in different organic solvents was conducted as shown further below to find a potential solvent able to dissolve the lignin polymers. Furthermore, the samples were filtered from any insoluble residue before SEC measurements to avoid clogging of the column. Also, at this step, the size of the detectable polymers is restricted by the pore size of the filter used. This would explain the detected, relatively low overall increase in molecular weight (Table 5). Therefore, the actual molecular weight at the later stages and the end point of the reaction is expected to be higher and the polymers themselves are likely not uniform in size. However, when the samples were analyzed by field flow fractionation (FFF), an alternative method to SEC, bigger molecules were detected in the unpolymerized and polymerized samples underlining the effects of filtering the samples prior to analysis. In the polymerized samples, polymers sizing up to 473 MD were detected. The FFF-MALLS chromatograms for LS and pLS are shown in the Supporting Information (Figures S3 and S4).

To characterize the structural changes occurring during the enzymatic LS polymerization reaction, we conducted an FTIR analysis was conducted. In the spectrum, the C−H stretching of the methoxy, methyl, and methylene groups in the side chains was observed (Figure 2).[54] Between 3000 and 2840 cm^{-1}, a sharper band is visible in the LS sample indicating the asymmetric stretching of C−H groups and fully saturated carbons such as $-CH_3$ and $-CH_2-$alkenes, while in the pLS, this band seemed broader, indicating the presence of −OH stretching and hydrogen-bonded carboxylic acid dimers. This can be an indicator for the incorporation of oxygen into LS, as assumed with elemental analysis, and the formation of the new bonds between the radicals.[16,55] General observations made in the FTIR spectrum are skeleton vibrations at 1600, 1514, and 1462 cm^{-1}, the C−H deformation, and aromatic ring vibrations at 1462 cm^{-1}. Furthermore, typical lignin units such as the characteristic bands of the G-ring and C=O stretch around 1270 cm^{-1} were well pronounced. At 1140

https://doi.org/10.1021/acssuschemeng.3c05521
ACS Sustainable Chem. Eng. XXXX, XXX, XXX−XXX

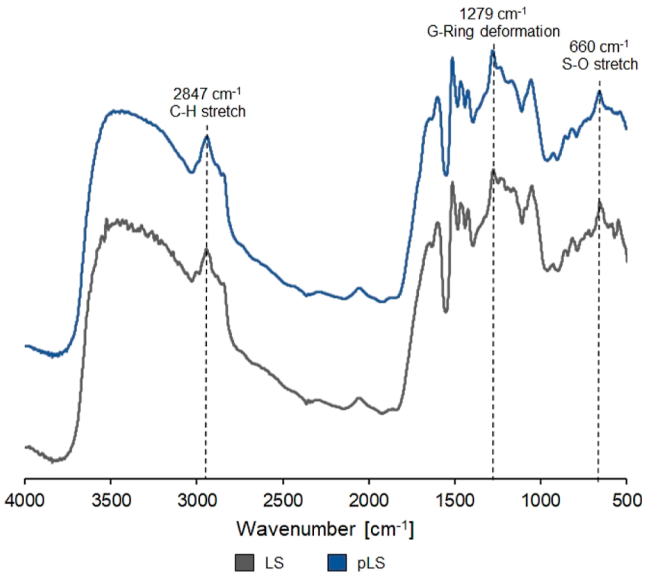

Figure 2. Comparison of the FTIR spectra of unpolymerized (LS, gray) to enzymatically polymerized LS (pLS, blue). The peaks at which the most relevant changes were determined are highlighted: C−H stretch was at 2847 cm^{-1}; G-ring deformation was at 1279 cm^{-1}; and the S−O stretch was at 660 cm^{-1}.

cm^{-1}, the C−H in-plane deformation and at 850 and 817 cm^{-1}, the C−H out-of-plane vibrations at positions 2, 5, and 6 of the G rings were found.[54] The S−O stretching vibration of the sulfonic groups can be observed between 660 and 620 cm^{-1} (Figure 2). Generally, the intensities in the pLS spectrum were found to be lower compared with those in the LS spectrum. This suggests decreasing amounts of the respective functional groups due to the formation of new interunit linkages during enzymatic polymerization. The signals of the G ring (around 1279 cm^{-1}) are decreasing because of the disruption of the aromatic character due to laccase-induced radicalization and the subsequent formation of quinone intermediates. Aside from that, new ether (β-O-4′, 4-O-5′) and C−C (5−5′) linkages are formed, leading to the observed decrease in intensity for pLS (Figure 2).[6,56,57]

To investigate these changes more closely, we conducted a 2D $^{1}H/^{13}C$ HSQC NMR analysis. Comparison of LS to pLS did not reveal significant differences in the aromatic regions except for lower intensities for pLS (Figure 3A,C). This was also evidenced in the FTIR spectra (Figure 2) and is due to the structural changes occurring during the enzymatic polymerization of LS, which were found to lead to lower signal intensities. A comparison of the aliphatic regions showed the appearance of new signals for pLS in the region from δ_C/δ_H 66/3.2 ppm to 66/3.5 ppm (Figure 3B,D). Signals appearing in this area are usually assigned to carbohydrate residues, specifically xylopyranose units.[58−60] However, these peaks were absent in the LS spectrum; thus, it was supposed that these signals originated from the added MtL. To prove this, an additional measurement of the enzyme was conducted. The obtained spectrum of the laccase showed the same peaks in this region, proving that these signals indeed originate from MtL (Figure 3E). The detailed HSQC spectrum of LS shows the typical signals for lignin (Figure 3A−D). In the aliphatic region, the signals for the usual interunit linkages are found. The methoxyl groups (OMe), $\beta-\beta$ (resinol) linkages (C), the β-aryl ether (β-O-4) linkages (A), and the phenylcumaran (β-5) linkages (B) assigned to the respective C atom (α, β, or γ) are highlighted (Figure 3B,D). Conversely, the typical signals of C_α-sulfonated motifs are not visible in the aliphatic region of both spectra.[61,62] This can probably be ascribed to the low solubility of these materials, especially after the enzymatic treatment, and may suggest that the soluble fraction does not contain a significant amount of sulfonated units. The aromatic part of the spectrum shows the typical signals for the G ring (G 2,5,6) as well as a weak signal for the S-ring (S 2,6) (Figure 3A,C). The used LS stems mainly from spruce, which belongs to softwood, thus comprising mainly of G-rings with a minor amount of H rings present.[63] Therefore, the observed strong signals for the G-ring were expected. Whereas the appearance of weak S-ring signals in the spectrum would not be expected for softwood lignin. However, the feed used for pulping is not pure spruce wood, but it is mixed with minor amounts of beech, which would explain the presence of the S-ring signals. Anyhow, the feed for pulping cannot be fully homogeneous concerning the age or the geographical region of the trees, and sometimes even minor parts of hardwoods may be present. Furthermore, it was shown that in some softwood species, minor amounts of S units can be present.[62,64] However, during NMR sample preparation, it turned out that pLS is difficult to solubilize completely, even in commonly used organic solvents. This may also be a reason for the observed weaker signals in the NMR spectrum of pLS. Thus, to be able to further analyze the insoluble pLS polymers, e.g., by NMR or MALDI-TOF, a suitable solvent must be found beforehand. Several studies handled this limitation by using additional solid-state analyses, such as NMR or MALDI-TOF to verify the findings made by the liquid methods.[57,65,66] Anyhow, for the pLS samples investigated, even these solid-state methods, especially MALDI-TOF, turned out to be inappropriate and thus were not considered for the structural characterization of pLS.

Another important property of polymer characterization is the thermal stability. One way to measure the thermal properties is presented by thermogravimetric analysis. Herein, the temperature of onset of degradation was found to be at around 145 °C (T_{onset}) and the temperature of the maximum degradation rate was determined at around 300 °C (T_{max}), with no significant differences between LS and pLS. Further, the residual mass at 900 °C was determined to be 31.4% for both samples. Slightly higher thermal stability was observed for pLS. This may be caused by the structural changes during polymerization where new C−C and C−O linkages are formed, which are known to be of higher thermal stability (Figure 4). Thermal degradation of LS is known to proceed in three stages (I−III), as can be observed in the TG and the DTG curves (Figure 4). In the first stage (I) up to 150 °C, mainly residual water and volatile compounds are evaporated. At this point, the onset temperature of degradation (T_{onset}) can be determined. During the second stage (II), main depolymerization and vitrification occur, in the region between approximately 150 and 450 °C. The β-O-4 linkages, which are of low thermal stability, are broken at lower temperatures, while with increasing temperatures, the C−C and C−O linkages are degraded. At this stage, weight loss appears at a high rate, thus the temperature of maximum degradation rate (T_{max}) typically lies within this region. In the third stage (III), further weight loss occurs but at a lower rate until the final temperature is reached and the residual mass can be determined.[67−69] Thermal degradation of LS leads to the formation of nonreactive carbon residues consisting mainly of

https://doi.org/10.1021/acssuschemeng.3c05521
ACS Sustainable Chem. Eng. XXXX, XXX, XXX−XXX

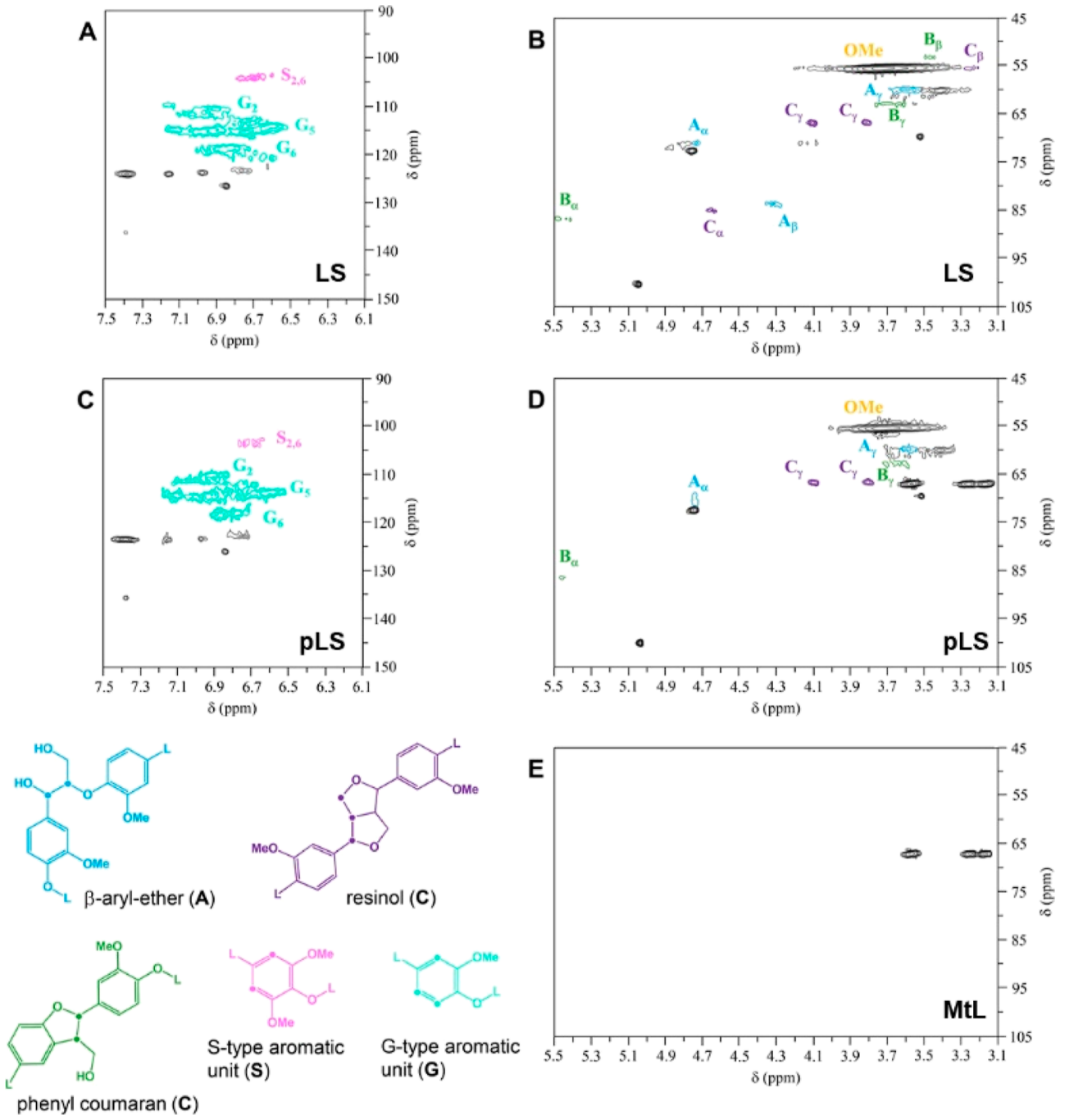

Figure 3. $^{1}H/^{13}C$ HSQC NMR spectra of LS and pLS. Shown are the aromatic (A,C) and aliphatic (B,D) regions and the aliphatic region for the MtL laccase enzyme (E). The most common structures found in lignin are presented and color-coded in the spectra.

aromatic rings, also known as char.[70,71] The herein obtained values are largely in accordance with literature, investigating the thermal decomposition of lignocellulosic biomass and lignin.[68,69,72] When comparing these results to other polymers, it turns out that the thermal stability obtained herein is low. Commonly used polymers, such as PS, PET, LDPE, PP, and PE, show onset temperatures ranging from 200 °C for PS up to 370 °C for PET. Also compared to other biobased polymers, such as PLA, PBS, or PIS (T_{onset} from 319 to 330 °C) it is lower. Consequently, the maximum degradation rate for the commercially available polymers also appears at higher temperatures. Further, degradation of pure and homologous polymers occurs in a single step and mostly results in lower residual mass.[73−76]

The specific heating capacities (c_p) of the samples were determined by differential scanning calorimetry (DSC) (Figure 5). To this end, the baselines of the measured heat flows of the samples and the reference material used (sapphire) were determined and used for the calculation of c_p. The graphs showed that LS and the lyophilized polymer films follow similar trends, while the granules were found to have slightly higher c_p values. The increase in heat capacity for the lyophilized pLS films can be attributed to reaching the temperature for the onset of degradation at around 145 °C, as determined by TGA (Figure 4). The higher c_p values for pLS

https://doi.org/10.1021/acssuschemeng.3c05521
ACS Sustainable Chem. Eng. XXXX, XXX, XXX−XXX

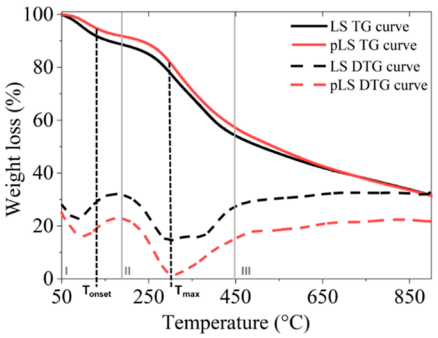

Figure 4. Comparison of the TGA (solid lines) and DTG (dashed lines) curves of LS (black) to pLS (red) after laccase-catalyzed polymerization. Shown are the temperatures where degradation starts (T_{onset}), the temperature where the highest degradation rate was reached (T_{max}), and the three stages of LS thermal degradation (I to III).

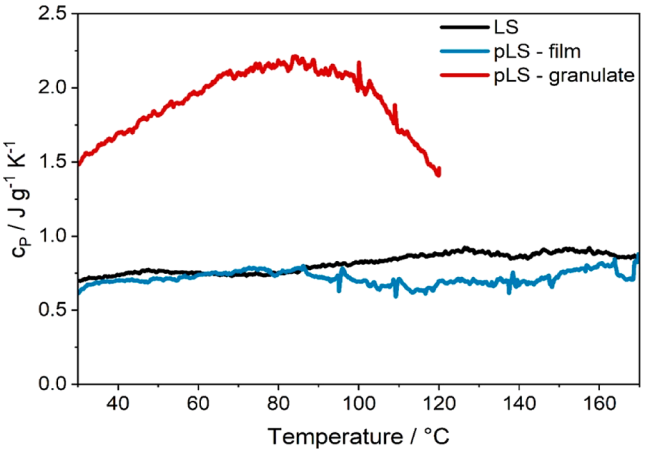

Figure 5. Results for the specific heating values (c_p) in a temperature range from 40 to 170 °C for LS (black), pLS lyophilized film (blue), and pLS granulate (red).

granulate can be explained by the higher amount of entrapped water present within, which would also explain the observed higher increase in heat capacity until 100 °C. Thereafter, it started to decrease because all water was evaporated. As shown by the structural analyses, the enzymatic polymerization of LS leads to the formation of new C−C and C−O bonds, which are of higher thermal stability. Thus, pLS showed slightly higher heat capacity than LS. Generally, the c_p value for the pLS granulate is in accordance with the literature.[77,78]

The polymerized material becomes insoluble in water, which makes it promising for various applications. However, as it turned out, it is also very resistant to organic solvents, hampering further characterization of the polymers. Thus, it would be interesting to find proper solvents that can dissolve pLS, to facilitate further analyses, such as MALDI-TOF. The swelling behavior of pLS in different formulations (films and granulates) was investigated by soaking them in organic solvents of different polarities (heptane, toluene, acetone, and isopropanol) at room temperature for 6 weeks. A weight gain of the polymer upon soaking in the respective solvent indicates diffusion of the solvent into the polymer, while a weight loss indicates polymer dissolution. Weight gain was determined by gravimetric analyses in triplicates. Standard deviations were below 0.1% (Figure 6).

Differences in solubility were observed for the films and granulates. The polar solvents acetone (polar aprotic) and isopropyl alcohol (polar protic) were found to partly dissolve pLS, independent of its formulation (either film or granulate). The films were found to be partially dissolved by both polar solvents since the mass of the polymer was reduced by nearly 40% within the first week while remaining nearly constant afterward. The effect was less pronounced in the granulate form, with only 6% weight loss after the first week. Moreover, after an initial partial dissolution, after 4 weeks, a new weight increase was observed for the polymer granulates immersed in acetone. This suggests that acetone first dissolves certain parts of the polymer, followed by swelling of the remaining polymer structure by 1%. The nonpolar solvents, hexane and toluene, were found to dissolve the films although to a lesser extent (4% in the case of toluene), while, at least in the beginning, both solvents were absorbed by the polymer in granulate form. In heptane, pLS films dissolved by 30% of their initial weight, but in contrast to the polar solvents, an extended mass decrease was observed during the entire runtime of the experiment. On the other hand, the polymer granulates exhibited signs of swelling within the first week of solvent uptake. However, in heptane, the granulates started to dissolve after the first week of soaking, while in toluene, dissolution was found to begin only after 2 weeks. In all the solvents tested, an insoluble residue was observed for both formulations at the end of the experiment (Figure 6A,B). The absolute weights of measured samples are reported in the Supporting Information (Tables S8 and S9).

The findings of the solvent uptake investigation suggest that pLS is more prone to dissolution in organic solvents in the form of films than as granulates. This may be because in granulates, the polymers are more densely packed, thus

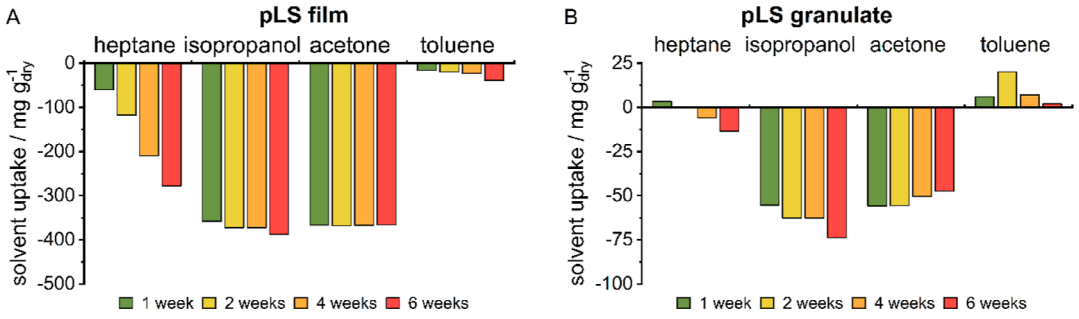

Figure 6. Solvent uptake by LS polymerized by laccase (pLS) in the form of flat films (A) and granulates (B) was monitored for a period of 6 weeks.

https://doi.org/10.1021/acssuschemeng.3c05521
ACS Sustainable Chem. Eng. XXXX, XXX, XXX−XXX

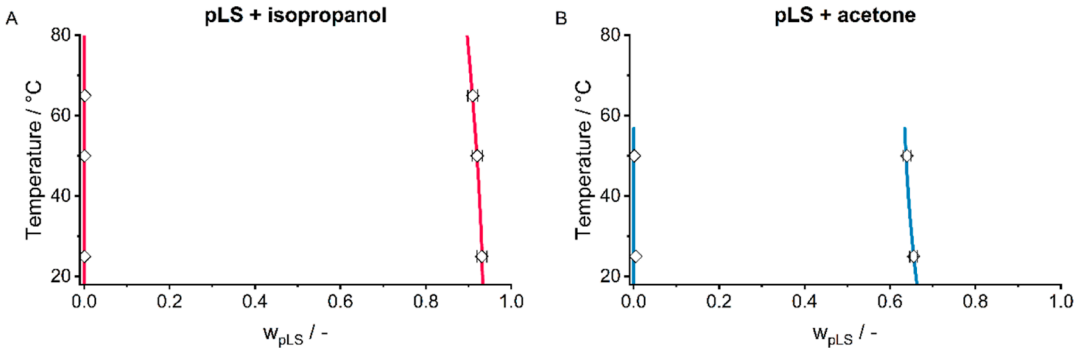

Figure 7. Liquid−liquid equilibrium of pLS + isopropanol (A) and pLS + acetone (B) determined in this work (symbols) and modeled with PC-SAFT (lines).

Table 6. PC-SAFT Model Parameters for the LS Polymer and Solvents: M: Molar Mass; m: Segment Number; σ: Segment Diameter; ϵ: Depth of Pair Potential; ϵ^{AB}: Association Energy; κ^{AB}: Association Volume; μ_D: Dipole Moment[a]

	M [g/mol]	m [-]	σ [Å]	ϵ/k_b [K]	ϵ^{AB} [K]	κ^{AB} [-]	μ_D[b] [D]	source
pLS	68.930	48.4	2.7599	237.61				this work
isopropanol	60.096	3.0929	3.2085	208.42	2253.9	0.0247		29
acetone	58.080	2.7147	3.2742	232.99			2.88	37

[a]Segment number of pLS is calculated by multiplication with its molecular weight as indicated. [b]Dipole moment: 1D = 3.33564 × 10^{-30} cm.

limiting mass transfer from the outside of the granulate to the inside, whereas in films, the functional side groups are presented on the outside facilitating the interaction with the solvents. In densely packed polymer granulates or spheres, the solvent first needs to diffuse into the polymer, followed by loosening the polymer structure indicated by swelling. Afterward, the chain disentanglement takes place resulting in the dissolution of the polymer.[79,80] This was observed for pLS granulates in heptane and toluene. On the other hand, acetone seems to quickly dissolve certain parts of the polymer granulate, while afterward it gets absorbed into the polymer network. Some studies on lignin solubility found that the solubility decreases with higher molecular weights and at higher aliphatic OH group content. This seems to be the case here, since upon enzymatic oxidation the phenolic OH concentration decreased, due to the formation of new interunit linkages (as also shown above by FTIR measurements), leading to an increase in aliphatic OH groups while simultaneously resulting in higher molecular weights.[81,82] Overall, the considerably lower dissolution by heptane and toluene suggests that pLS is significantly more resistant to nonpolar solvents. This is a further indicator of the abundance of polar functional groups after polymerization, which remain from the LS precursor. Moreover, the dissolution of the pLS film in isopropanol and acetone to a constant equilibrium value after 1 week (Figure 6A) indicates a demixing region between pLS and these two solvents, thereby forming a polymer−solvent liquid−liquid equilibrium (LLE) under the investigated conditions. The solubility of the solvents in equilibrium samples of pLS was therefore determined by evaporation of the solvent at T = 100 °C for 1 week and determination of the mass difference before and after evaporation. The decrease in mass directly corresponds to the amount of solvent contained in the polymer in equilibrium, thereby enabling the calculation of the equilibrium mass fractions in the polymer-rich phase based on the dry mass of the polymer. Regarding the solvent-rich phase, while nearly 40% mass loss of the polymer was observed in solvent uptake experiments, this could only be achieved in large excess quantities of the respective solvents ($m_{solvent}/m_{pLS} \sim 10^3$)—but no measurable residue of pLS in the solvent phase could be detected. However, since the dry mass of the polymer was determined before and after the LLE experiments, the content of dissolved pLS in the respective solvent phase was calculated via a simple mass balance. In addition to room temperature experiments, solvent solubilities were also determined at T = 50 °C (isopropanol, acetone) and T = 65 °C (isopropanol) at ambient pressure to determine the dependency of solvent solubilities on temperature. Hence, five points of the isobaric LLE of pLS + 2-propanol and pLS + acetone in the polymer-rich phase could be determined (Figure 7). The experimental LLE data was then used to parametrize the PC-SAFT model. Thereby, pure-component parameters of pLS were adjusted to experimental density measurements and the respective solubilities of isopropanol and acetone. The parameter adjustment approach is similar to the regression method used by Krenn et al.[32] for cross-linked epoxy resins, where pure-component polymer parameters were adjusted to the solvent uptake of polymers. To reduce the number of adjustable parameters, no self-association or polar interaction was considered for pLS. Furthermore, pLS is modeled as a monodisperse polymer, with the first moment of its distribution, i.e., the number-average molecular weight M_n (Table 5), serving as the molecular weight parameter for PC-SAFT (Table 6). Since calorimetric investigations (TGA/DTA, Figure 4 and DSC, Figure 5) revealed no phase transitions above the room temperature of pLS, an amorphous state above the glass transition temperature is assumed for the modeling approach of the polymer. The adjusted parameter set for pLS was applied; the liquid density of the pLS film was modeled in exceptional accordance with experimental data, exhibiting a deviation of only 1.82% (Table 7).

However, the calculation of the density with PC-SAFT was found to be reliable only for the film, with the granulate formulation exhibiting an 11.6% lower density compared to the model. This can be attributed to the difference in residual water content between the polymer film and granulate, which is not considered by the modeling approach. For binary LLEs of pLS and solvents, the binary interaction parameter k_{ij} for

https://doi.org/10.1021/acssuschemeng.3c05521
ACS Sustainable Chem. Eng. XXXX, XXX, XXX−XXX

Table 7. Experimental and Calculated (PC-SAFT) Density at T = 25 °C of pLS Film and Granulate Formulations

	density exp. [kg/m^3]	density PC-SAFT [kg/m^3]	deviation [%]
film	1392.07	1417.42	1.82
granulate	1270.64	1417.42	11.55

unlike segment interactions in the PC-SAFT framework was adjusted to experimental solubility data of isopropanol and acetone in pLS at ambient pressure, as demonstrated previously by Krenn et al.[32] for epoxy resins. Pure-component parameters of solvents were taken from the literature, and all pure-component model parameters are reported alongside the pLS parameters adjusted in this work in Table 6. Modeled phase equilibria of pLS + 2-propanol and pLS + acetone are depicted in Figure 7 and compared to experimental solubility data. For isopropanol, a temperature-dependent interaction parameter (eq 3) was found to be adequate for modeling the solubility in pLS, thereby yielding highly accurate results (Figure 7A). Conversely, a constant binary interaction parameter of k_{ij} = −0.015 was found to be sufficient to describe the solubility of acetone in pLS in remarkable accordance with the experimental data (Figure 7B). All binary interaction parameters are listed in Table 8. The predictability

Table 8. Binary Interaction Parameters Determined in This Work (Eq 3)

i	j	k_{ij}^{a} [-]	k_{ij}^{b} [K]
pLS	isopropanol	−0.0066	3.88 × 10−5
pLS	acetone	−0.0149	0

of the model could feasibly be improved in subsequent investigations of pLS systems by incorporating free association sites[83] of the lignin units, and by considering the polydispersity of the polymer. The polydispersity can be accounted for by dividing the polymer into multiple pseudocomponents, with molar weights based on the first, second, and third moment (i.e., M_n, M_w, and M_z) of the molecular weight distribution, as demonstrated by Tork et al.[84]

$$k_{ij} = k_{ij}^{a} + \frac{k_{ij}^{b}}{T} \quad (3)$$

4. CONCLUSIONS

Laccase-catalyzed polymerization of LS was investigated by structural and thermal analyses. Based on the mass balance and elemental analyses, it was possible to elaborate a reaction equation. This enabled us further to determine the enthalpy of the reaction, which was found to be −60.84 kJ/kg$_{feed}$ indicating that the reaction is slightly exothermic overall. Thorough analyses and characterization of LS and pLS revealed that there are only minor changes in the molecular structure of LS, which was also proven by the reaction equation. The phenolic hydrogen content of LS decreased due to abstraction of the hydrogen atom and subsequent formation of water, while the oxygen content increased upon laccase treatment, which was found to be upon nonenzymatic incorporation of oxygen into the LS molecules. The analytical methods further revealed that the conditions chosen for the enzymatic polymerization of LS led only to the wanted increases in molecular weight and viscosity since no or only minor signs of other reactions could have been determined. Oxidation of LS leads to a decrease in the aromatic character and the formation of new C−C and C−O bonds between the radical intermediates. However, although enzyme-catalyzed polymerization of LS led to only a slight increase in the thermal stability of pLS, the observed minor structural changes led to big impacts on pLS properties, such as insolubility in water and reduced solubility in organic solvents, with an insoluble residue of polymerized LS found in each of the solvents tested. Further, it was shown that the description of the dissolution behavior of pLS films in organic solvents by the PC-SAFT model was reliable, while it was not applicable for pLS granulates due to the remaining water content. With the results gathered herein, it is possible to describe the enzymatic polymerization of LS in more detail, allowing for better predictions of the reaction outcome, and with the proven solubility prediction model, it will be possible to search for an appropriate solvent to dissolve pLS, allowing further structural analyses.

■ ASSOCIATED CONTENT

Supporting Information

The Supporting Information is available free of charge at https://pubs.acs.org/doi/10.1021/acssuschemeng.3c05521.

Overview of the reaction conditions and setup; detailed results for the mass balance, dry substance determination, reaction progress monitoring, and dissolution experiments; and SEC-MALLS and FFF-MALLS chromatograms (PDF)

■ AUTHOR INFORMATION

Corresponding Author

Renate Weiss − *Department of Agrobiotechnology, IFA-Tulln, Institute of Environmental Biotechnology, University of Natural Resources and Life Sciences, Vienna, 3430 Tulln an der Donau, Austria;* orcid.org/0000-0001-7680-9832; Email: renate.weiss@boku.ac.at

Authors

Sebastian A. Mayr − *Department of Agrobiotechnology, IFA-Tulln, Institute of Environmental Biotechnology, University of Natural Resources and Life Sciences, Vienna, 3430 Tulln an der Donau, Austria;* orcid.org/0000-0001-6319-9908

Stefan Wagner − *Institute of Chemical Engineering and Environmental Technology, Graz University of Technology, 8010 Graz, Austria*

Roland Nagl − *Institute of Chemical Engineering and Environmental Technology, Graz University of Technology, 8010 Graz, Austria*

Alessandro Pellis − *Department of Chemistry and Industrial Chemistry, University of Genova, 16146 Genova, Italy*

Matteo Gigli − *Department of Molecular Sciences and Nanosystems, Ca' Foscari University of Venice, 30172 Venezia Mestre (VE), Italy;* orcid.org/0000-0003-3899-0399

Claudia Crestini − *Department of Molecular Sciences and Nanosystems, Ca' Foscari University of Venice, 30172 Venezia Mestre (VE), Italy;* orcid.org/0000-0001-9903-2675

Melissa Horvat − *Sappi Papier Holding GmbH, 8101 Gratkorn, Austria*

https://doi.org/10.1021/acssuschemeng.3c05521
ACS Sustainable Chem. Eng. XXXX, XXX, XXX−XXX

Tim Zeiner − *Institute of Chemical Engineering and Environmental Technology, Graz University of Technology, 8010 Graz, Austria;* orcid.org/0000-0001-7298-4828
Georg M. Guebitz − *Department of Agrobiotechnology, IFA-Tulln, Institute of Environmental Biotechnology, University of Natural Resources and Life Sciences, Vienna, 3430 Tulln an der Donau, Austria; Austrian Centre for Industrial Biotechnology (ACIB), 3430 Tulln, Austria*
Nikolaus Schwaiger − *Sappi Papier Holding GmbH, 8101 Gratkorn, Austria*

Complete contact information is available at: https://pubs.acs.org/10.1021/acssuschemeng.3c05521

Author Contributions

Conceptualization, G.M.G., N.S., R.N., R.W.; methodology, N.S., R.W.; validation, S.A.M., N.S., R.W., R.N., A.P., M.G., T.Z., S.W., M.H.; formal analysis, S.A.M., R.W.; investigation, S.A.M., R.W., N.S., R.N., M.G., A.P., T.Z., S.W., M.H.; resources, G.M.G., N.S., R.W.; writing—original draft preparation, S.A.M., R.W.; writing—review and editing, all authors; visualization, S.A.M., G.M.G., N.S., R.W., R.N., A.P., M.G.; supervision, G.M.G., N.S., R.W., C.C.; project administration, R.W., G.M.G., S.A.M.; funding acquisition, R.W., G.M.G., N.S. All authors have read and agreed to the published version of the manuscript.

Funding

The SUSFERT project has received funding from the Biobased Industries Joint Undertaking (BBI-JU) under grant agreement no. 792021. The BBI-JU receives support from the European Union's Horizon 2020 research and innovation program and the Bio-Based Industries Consortium.

Notes

The authors declare no competing financial interest.

■ ACKNOWLEDGMENTS

The authors extend their gratitude to Julija Strunčnik and Lara Schönbacher for their support in the lab and to Sara Mayr-Güley for her help with the finalization of the supplementary cover image. Open-access funding was provided by the University of Natural Resources and Life Sciences Vienna (BOKU).

■ REFERENCES

(1) Nikolaou, I. E.; Jones, N.; Stefanakis, A. Correction to: Circular Economy and Sustainability: The Past, the Present and the Future Directions. *Circ. Econ. Sustainability* **2021**, *1* (2), 783.
(2) Ragauskas, A. J.; Williams, C. K.; Davison, B. H.; Britovsek, G.; Cairney, J.; Eckert, C. A.; Frederick, W. J.; Hallett, J. P.; Leak, D. J.; Liotta, C. L.; Mielenz, J. R.; Murphy, R.; Templer, R.; Tschaplinski, T. The Path Forward for Biofuels and Biomaterials. *Science* **2006**, *311*, 484−489.
(3) Schutyser, W.; Renders, T.; Van Den Bosch, S.; Koelewijn, S. F.; Beckham, G. T.; Sels, B. F. Chemicals from Lignin: An Interplay of Lignocellulose Fractionation, Depolymerisation, and Upgrading. *Chem. Soc. Rev.* **2018**, *47* (3), 852−908.
(4) Calvo-Flores, F. G.; Dobado, J. A. Lignin as Renewable Raw Material. *ChemSusChem* **2010**, *3* (11), 1227−1235.
(5) Gil-Chávez, J.; Gurikov, P.; Hu, X.; Meyer, R.; Reynolds, W.; Smirnova, I. Application of Novel and Technical Lignins in Food and Pharmaceutical Industries: Structure-Function Relationship and Current Challenges. *Biomass Convers. Biorefin.* **2021**, *11*, 2387−2403.
(6) Agustin, M. B.; de Carvalho, D. M.; Lahtinen, M. H.; Hilden, K.; Lundell, T.; Mikkonen, K. S. Laccase as a Tool in Building Advanced Lignin-Based Materials. *ChemSusChem* **2021**, *14* (21), 4615−4635.
(7) Morozova, O. V.; Shumakovich, G. P.; Gorbacheva, M. A.; Shleev, S. V.; Yaropolov, A. I. "Blue" laccases. *Biochemistry* **2007**, *72* (10), 1136−1150.
(8) Baldrian, P. Fungal Laccases-Occurrence and Properties. *FEMS Microbiol. Rev.* **2006**, *30* (2), 215−242.
(9) Mayr, S. A.; Schwaiger, N.; Weber, H. K.; Kovač, J.; Guebitz, G. M.; Nyanhongo, G. S. Enzyme Catalyzed Copolymerization of Lignosulfonates for Hydrophobic Coatings. *Front. Bioeng. Biotechnol.* **2021**, *9*, 697310.
(10) Sitarz, A. K.; Mikkelsen, J. D.; Meyer, A. S. Structure, Functionality and Tuning up of Laccases for Lignocellulose and Other Industrial Applications. *Crit. Rev. Biotechnol.* **2016**, *36* (1), 70−86.
(11) Madhavi, V.; Lele, S. S. Laccase: Properties and Applications. *Bioresources* **2009**, *4*, 1694.
(12) Hahn, V.; Mikolasch, A.; Schauer, F. Cleavage and Synthesis Function of High and Low Redox Potential Laccases towards 4-Morpholinoaniline and Aminated as Well as Chlorinated Phenols. *Appl. Microbiol. Biotechnol.* **2014**, *98* (4), 1609−1620.
(13) Singh, B. Myceliophthora Thermophila Syn. Sporotrichum Thermophile: A Thermophilic Mould of Biotechnological Potential. *Crit. Rev. Biotechnol.* **2016**, *36* (1), 59−69.
(14) Huber, D.; Ortner, A.; Daxbacher, A.; Nyanhongo, G. S.; Bauer, W.; Guebitz, G. M. Influence of Oxygen and Mediators on Laccase-Catalyzed Polymerization of Lignosulfonate. *ACS Sustain. Chem. Eng.* **2016**, *4* (10), 5303−5310.
(15) Ortner, A.; Huber, D.; Haske-Cornelius, O.; Weber, H. K.; Hofer, K.; Bauer, W.; Nyanhongo, G. S.; Guebitz, G. M. Laccase Mediated Oxidation of Industrial Lignins: Is Oxygen Limiting? *Process Biochem.* **2015**, *50* (8), 1277−1283.
(16) Weiss, R.; Ghitti, E.; Sumetzberger-Hasinger, M.; Guebitz, G. M.; Nyanhongo, G. S. Lignin-Based Pesticide Delivery System. *ACS Omega* **2020**, *5* (8), 4322−4329.
(17) Braunschmid, V.; Binder, K.; Fuerst, S.; Subagia, R.; Danner, C.; Weber, H.; Schwaiger, N.; Nyanhongo, G. S.; Ribitsch, D.; Guebitz, G. M. Comparison of a Fungal and a Bacterial Laccase for Lignosulfonate Polymerization. *Process Biochem.* **2021**, *109*, 207−213.
(18) Padhi, S. S. P.; Jimenez Bartolome, M.; Nyanhongo, G. S.; Schwaiger, N.; Pellis, A.; Van Herwijnen, H. W. G.; Guebitz, G. M. Role of Surface Enhancement in the Enzymatic Cross-Linking of Lignosulfonate Using Alternative Downstream Techniques. *ACS Omega* **2022**, *7* (27), 23749−23758.
(19) Mayr, S. A.; Subagia, R.; Weiss, R.; Schwaiger, N.; Weber, H. K.; Leitner, J.; Ribitsch, D.; Nyanhongo, G. S.; Guebitz, G. M. Oxidation of Various Kraft Lignins with a Bacterial Laccase Enzyme. *Int. J. Mol. Sci.* **2021**, *22* (23), 13161.
(20) Huber, D.; Pellis, A.; Daxbacher, A.; Nyanhongo, G. S.; Guebitz, G. M. Polymerization of Various Lignins via Immobilized Myceliophthora Thermophila Laccase (MtL). *Polymers* **2016**, *8* (8), 280.
(21) Nyanhongo, G. S.; Guebitz, G. M.; Ortner, A.; Bischof, S. Verfahren Zur Herstellung Eines Lignosulfonat-Polymers. WO 2020152314 A1, 2020.
(22) Weiß, R.; Gritsch, S.; Brader, G.; Nikolic, B.; Spiller, M.; Santolin, J.; Weber, H. K.; Schwaiger, N.; Pluchon, S.; Dietel, K.; Gübitz, G.; Nyanhongo, G. A Biobased, Bioactive, Low CO2impact Coating for Soil Improvers. *Green Chem.* **2021**, *23* (17), 6501−6514.
(23) Hellmayr, R.; Bischof, S.; Wühl, J.; Guebitz, G. M.; Nyanhongo, G. S.; Schwaiger, N.; Liebner, F.; Wimmer, R. Enzymatic Conversion of Lignosulfonate into Wood Adhesives: A Next Step towards Fully Biobased Composite Materials. **2022**. .
(24) Jimenez Bartolome, M.; Padhi, S. S. P.; Fichtberger, O. G.; Schwaiger, N.; Seidl, B.; Kozich, M.; Nyanhongo, G. S.; Guebitz, G. M. Improving Properties of Starch-Based Adhesives with Carboxylic Acids and Enzymatically Polymerized Lignosulfonates. *Int. J. Mol. Sci.* **2022**, *23* (21), 13547.
(25) Jimenez Bartolome, M.; Bischof, S.; Pellis, A.; Konnerth, J.; Wimmer, R.; Weber, H.; Schwaiger, N.; Guebitz, G. M.; Nyanhongo, G. S. Enzymatic Synthesis and Tailoring Lignin Properties: A

Systematic Study on the Effects of Plasticizers. *Polymer* **2020**, *202*, 122725.
(26) Ortner, A.; Hofer, K.; Bauer, W.; Nyanhongo, G. S.; Guebitz, G. M. Laccase Modified Lignosulfonates as Novel Binder in Pigment Based Paper Coating Formulations. *React. Funct. Polym.* **2018**, *123*, 20−25.
(27) Sette, M.; Wechselberger, R.; Crestini, C. Elucidation of Lignin Structure by Quantitative 2D NMR. *Chem.—Eur. J.* **2011**, *17* (34), 9529−9535.
(28) Gross, J.; Sadowski, G. Perturbed-Chain SAFT: An Equation of State Based on a Perturbation Theory for Chain Molecules. *Ind. Eng. Chem. Res.* **2001**, *40* (4), 1244−1260.
(29) Gross, J.; Sadowski, G. Application of the Perturbed-Chain SAFT Equation of State to Associating Systems. *Ind. Eng. Chem. Res.* **2002**, *41* (22), 5510−5515.
(30) Gross, J.; Sadowski, G. Modeling Polymer Systems Using the Perturbed-Chain Statistical Associating Fluid Theory Equation of State. *Ind. Eng. Chem. Res.* **2002**, *41* (5), 1084−1093.
(31) Tumakaka, F.; Gross, J.; Sadowski, G. Modeling of Polymer Phase Equilibria Using Perturbed-Chain SAFT. *Fluid Phase Equilib.* **2002**, *194*−*197*, 541−551.
(32) Krenn, P.; Zimmermann, P.; Fischlschweiger, M.; Zeiner, T. Modeling Liquid Absorption of Highly Cross-Linked Epoxy Resins in Aqueous Electrolyte Solutions. *Fluid Phase Equilib.* **2021**, *529*, 112881.
(33) Tumakaka, F.; Gross, J.; Sadowski, G. Thermodynamic Modeling of Complex Systems Using PC-SAFT. *Fluid Phase Equilib.* **2005**, *228*−*229*, 89−98.
(34) Walowski, C.; Langenbach, K.; Browarzik, D.; Enders, S. Cloud Point Pressure in the System Polyethylene + Ethylene - Impact of Branching. *Fluid Phase Equilib.* **2016**, *428*, 38−47.
(35) Hübner, M.; Lodziak, C.; Do, H. T. J.; Held, C. Measuring and Modeling Thermodynamic Properties of Aqueous Lysozyme and BSA Solutions. *Fluid Phase Equilib.* **2018**, *472*, 62−74.
(36) Voges, M.; Herhut, M.; Held, C.; Brandenbusch, C. Light-Scattering Data of Protein and Polymer Solutions: A New Approach for Model Validation and Parameter Estimation. *Fluid Phase Equilib.* **2018**, *465*, 65−72.
(37) Gross, J.; Vrabec, J. An Equation-of-State Contribution for Polar Components: Dipolar Molecules. *AIChE J.* **2006**, *52* (3), 1194−1204.
(38) Arndt, M. C.; Sadowski, G. Modeling Poly(N-Isopropylacrylamide) Hydrogels in Water/Alcohol Mixtures with PC-SAFT. *Macromolecules* **2012**, *45* (16), 6686−6696.
(39) Krenn, P.; Zimmermann, P.; Fischlschweiger, M.; Zeiner, T. SAFT-Based Maxwell-Stefan Approach to Model the Diffusion through Epoxy Resins. *J. Chem. Eng. Data* **2020**, *65* (12), 5677−5687.
(40) Miao, B.; Vilgis, T. A.; Poggendorf, S.; Sadowski, G. Effect of Finite Extensibility on the Equilibrium Chain Size. *Macromol. Theory Simul.* **2010**, *19* (7), 414−420.
(41) Jones, S. M.; Solomon, E. I. Electron Transfer and Reaction Mechanism of Laccases. *Cell. Mol. Life Sci.* **2015**, *72* (5), 869−883.
(42) Atkins, P.; Paula, J. de. *Atkins' Physical Chemistry*, 8th ed.; Oxford University Press, 2006; pp 40−60.
(43) Khattak, R.; Sayed, M.; Sufaid Khan, M.; Noreen, H. Introductory Chapter: Redox—An Overview. *Redox*, 2020; IntechOpen..
(44) Kalliola, A.; Kuitunen, S.; Liitiä, T.; Rovio, S.; Ohra-Aho, T.; Vuorinen, T.; Tamminen, T. Lignin Oxidation Mechanisms under Oxygen Delignification Conditions. Part 1. Results from Direct Analyses. *Holzforschung* **2011**, *65* (4), 567−574.
(45) Capanema, E. A.; Balakshin, M. Y.; Chen, C. L.; Gratzl, J. S.; Kirkman, A. G. Oxidative Ammonolysis of Technical Lignins Part 2. Effect of Oxygen Pressure. *Holzforschung* **2001**, *55* (4), 405−412.
(46) Velázquez-Martí, B.; López-Cortés, I.; Salazar-Hernández, D.; Callejón-Ferre, Á. J. Modeling the Calorific Value of Biomass from Fruit Trees Using Elemental Analysis Data. *Biomass Volume Estimation and Valorization for Energy* 2017; IntechOpen..
(47) Peduzzi, E.; Boissonnet, G.; Maréchal, F. Biomass Modelling: Estimating Thermodynamic Properties from the Elemental Composition. *Fuel* **2016**, *181*, 207−217.
(48) Sheng, C.; Azevedo, J. L. T. Estimating the Higher Heating Value of Biomass Fuels from Basic Analysis Data. *Biomass Bioenergy* **2005**, *28* (5), 499−507.
(49) Jenkins, B. M.; Baxter, L. L.; Miles, T. R.; Miles, T. R. Combustion Properties of Biomass. *Fuel Process. Technol.* **1998**, *54* (1−3), 17−46.
(50) Zeigler, H. P.; Schmerler, S. Visual Discrimination of Orientation by Pigeons. *Anim. Behav.* **1965**, *13* (4), 475−477.
(51) Pecchi, M.; Basso, D.; Patuzzi, F.; Baratieri, M. Effect of Water Formation on the Reaction Enthalpy of the Hydrothermal Carbonization Process. *European Biomass Conference and Exhibition*, 2019; pp 1155−1159.
(52) Perna, V.; Agger, J. W.; Andersen, M. L.; Holck, J.; Meyer, A. S. Laccase Induced Lignin Radical Formation Kinetics Evaluated by Electron Paramagnetic Resonance Spectroscopy. *ACS Sustain. Chem. Eng.* **2019**, *7* (12), 10425−10434.
(53) Giardina, P.; Faraco, V.; Pezzella, C.; Piscitelli, A.; Vanhulle, S.; Sannia, G. Laccases: A Never-Ending Story. *Cell. Mol. Life Sci.* **2010**, *67* (3), 369−385.
(54) Boeriu, C. G.; Bravo, D.; Gosselink, R. J. A.; Van Dam, J. E. G. Characterisation of Structure-Dependent Functional Properties of Lignin with Infrared Spectroscopy. *Ind. Crops Prod.* **2004**, *20* (2), 205−218.
(55) Lisperguer, J.; Perez, P.; Urizar, S. Structure and Thermal Properties of Lignins: Characterization by Infrared Spectroscopy and Differential Scanning Calorimetry. *J. Chil. Chem. Soc.* **2009**, *54* (4), 460−463.
(56) Zavada, S. R.; Battsengel, T.; Scott, T. F. Radical-Mediated Enzymatic Polymerizations. *Int. J. Mol. Sci.* **2016**, *17* (2), 195.
(57) Nugroho Prasetyo, E.; Kudanga, T.; Østergaard, L.; Rencoret, J.; Gutiérrez, A.; del Río, J. C.; Ignacio Santos, J.; Nieto, L.; Jiménez-Barbero, J.; Martínez, A. T.; Li, J.; Gellerstedt, G.; Lepifre, S.; Silva, C.; Kim, S. Y.; Cavaco-Paulo, A.; Seljebakken Klausen, B.; Lutnaes, B. F.; Nyanhongo, G. S.; Guebitz, G. M. Polymerization of Lignosulfonates by the Laccase-HBT (1-Hydroxybenzotriazole) System Improves Dispersibility. *Bioresour. Technol.* **2010**, *101* (14), 5054−5062.
(58) Rencoret, J.; Pereira, A.; Marques, G.; del Río, J. C.; Martínez, Á. T.; Gutiérrez, A. A Commercial Laccase-Mediator System to Delignify and Improve Saccharification of the Fast-Growing Paulownia Fortunei (Seem.) Hemsl. *Holzforschung* **2018**, *73* (1), 45−54.
(59) Rencoret, J.; Pereira, A.; del Río, J. C.; Martínez, A. T.; Gutiérrez, A. Laccase-Mediator Pretreatment of Wheat Straw Degrades Lignin and Improves Saccharification. *BioEnergy Res.* **2016**, *9* (3), 917−930.
(60) Fasching, M.; Schröder, P.; Wollboldt, R. P.; Weber, H. K.; Sixta, H. A New and Facile Method for Isolation of Lignin from Wood Based on Complete Wood Dissolution. *Holzforschung* **2008**, *62* (1), 15−23.
(61) Marques, A. P.; Evtuguin, D. V.; Magina, S.; Amado, F. M. L.; Prates, A. Structure of Lignosulphonates from Acidic Magnesium-Based Sulphite Pulping of Eucalyptus Globulus. *J. Wood Chem. Technol.* **2009**, *29* (4), 337−357.
(62) Musl, O.; Sulaeva, I.; Bacher, M.; Mahler, A. K.; Rosenau, T.; Potthast, A. Hydrophobic Interaction Chromatography in 2 D Liquid Chromatography Characterization of Lignosulfonates. *ChemSusChem* **2020**, *13* (17), 4595−4604.
(63) Liu, X.; Bouxin, F. P.; Fan, J.; Budarin, V. L.; Hu, C.; Clark, J. H. Recent Advances in the Catalytic Depolymerization of Lignin towards Phenolic Chemicals: A Review. *ChemSusChem* **2020**, *13* (17), 4296−4317.
(64) Faleva, A. V.; Kozhevnikov, A. Y.; Pokryshkin, S. A.; Falev, D. I.; Shestakov, S. L.; Popova, J. A. Structural Characteristics of Different Softwood Lignins According to 1D and 2D NMR Spectroscopy. *J. Wood Chem. Technol.* **2020**, *40* (3), 178−189.

https://doi.org/10.1021/acssuschemeng.3c05521
ACS Sustainable Chem. Eng. XXXX, XXX, XXX−XXX

(65) García-Fuentevilla, L.; Domínguez, G.; Martín-Sampedro, R.; Hernández, M.; Arias, M. E.; Santos, J. I.; Ibarra, D.; Eugenio, M. E. Enzyme-Catalyzed Polymerization of Kraft Lignin from Eucalyptus Globulus: Comparison of Bacterial and Fungal Laccases Efficacy. *Polymers* **2023**, *15* (3), 513.
(66) Ibarra, D.; García-Fuentevilla, L.; Domínguez, G.; Martín-Sampedro, R.; Hernández, M.; Arias, M. E.; Santos, J. I.; Eugenio, M. E. NMR Study on Laccase Polymerization of Kraft Lignin Using Different Enzymes Source. *Int. J. Mol. Sci.* **2023**, *24* (3), 2359.
(67) Tian, R.; Liu, Q.; Zhang, W.; Zhang, Y. Preparation of Lignin-Based Hydrogel and Its Adsorption on Cu2+ Ions and Co2+ Ions in Wastewaters. *J. Inorg. Organomet. Polym. Mater.* **2018**, *28* (6), 2545−2553.
(68) Singh, Y. D.; Mahanta, P.; Bora, U. Comprehensive Characterization of Lignocellulosic Biomass through Proximate, Ultimate and Compositional Analysis for Bioenergy Production. *Renewable Energy* **2017**, *103*, 490−500.
(69) Gordobil, O.; Moriana, R.; Zhang, L.; Labidi, J.; Sevastyanova, O. Assesment of Technical Lignins for Uses in Biofuels and Biomaterials: Structure-Related Properties, Proximate Analysis and Chemical Modification. *Ind. Crops Prod.* **2016**, *83*, 155−165.
(70) Hu, X.; Gholizadeh, M. Biomass Pyrolysis: A Review of the Process Development and Challenges from Initial Researches up to the Commercialisation Stage. *J. Energy Chem.* **2019**, *39* (x), 109−143.
(71) Yang, H.; Dong, Z.; Liu, B.; Chen, Y.; Gong, M.; Li, S.; Chen, H. A New Insight of Lignin Pyrolysis Mechanism Based on Functional Group Evolutions of Solid Char. *Fuel* **2021**, *288*, 119719.
(72) Hemmilä, V.; Hosseinpourpia, R.; Adamopoulos, S.; Eceiza, A. Characterization of Wood-Based Industrial Biorefinery Lignosulfonates and Supercritical Water Hydrolysis Lignin. *Waste Biomass Valorization* **2020**, *11* (11), 5835−5845.
(73) Yang, J.; Miranda, R.; Roy, C. Using the DTG Curve Fitting Method to Determine the Apparent Kinetic Parameters of Thermal Decomposition of Polymers. *Polym. Degrad. Stab.* **2001**, *73* (3), 455−461.
(74) Singh, S.; Patil, T.; Tekade, S. P.; Gawande, M. B.; Sawarkar, A. N. Studies on Individual Pyrolysis and Co-Pyrolysis of Corn Cob and Polyethylene: Thermal Degradation Behavior, Possible Synergism, Kinetics, and Thermodynamic Analysis. *Sci. Total Environ.* **2021**, *783*, 147004.
(75) Das, P.; Tiwari, P. Thermal Degradation Kinetics of Plastics and Model Selection. *Thermochim. Acta* **2017**, *654*, 191−202.
(76) Qi, J.; Wu, J.; Chen, J.; Wang, H. An Investigation of the Thermal and (Bio)Degradability of PBS Copolyesters Based on Isosorbide. *Polym. Degrad. Stab.* **2019**, *160*, 229−241.
(77) Voitkevich, O. V.; Kabo, G. J.; Blokhin, A. V.; Paulechka, Y. U.; Shishonok, M. V. Thermodynamic Properties of Plant Biomass Components. Heat Capacity, Combustion Energy, and Gasification Equilibria of Lignin. *J. Chem. Eng. Data* **2012**, *57* (7), 1903−1909.
(78) Wang, J.; Hou, S.; Shen, Z.; Wen, J.; Qi, C. Thermal Characteristics and Simulation of Enzymatic Lignin Isolated from Chinese Fir and Birch. *Forests* **2022**, *13* (6), 914.
(79) Miller-Chou, B. A.; Koenig, J. L. A Review of Polymer Dissolution. *Prog. Polym. Sci.* **2003**, *28* (8), 1223−1270.
(80) Kappert, E. J.; Raaijmakers, M. J. T.; Tempelman, K.; Cuperus, F. P.; Ogieglo, W.; Benes, N. E. Swelling of 9 Polymers Commonly Employed for Solvent-Resistant Nanofiltration Membranes: A Comprehensive Dataset. *J. Membr. Sci.* **2019**, *569*, 177−199.
(81) Sameni, J.; Krigstin, S.; Sain, M. Solubility of Lignin and Acetylated Lignin in Organic Solvents. *Bioresources* **2017**, *12* (1), 1548−1565.
(82) Sadeghifar, H.; Ragauskas, A. Perspective on Technical Lignin Fractionation. *ACS Sustain. Chem. Eng.* **2020**, *8* (22), 8086−8101.
(83) Huang, S. H.; Radosz, M. Equation of State for Small, Large, Polydisperse, and Associating Molecules: Extension to Fluid Mixtures. *Ind. Eng. Chem. Res.* **1991**, *30* (8), 1994−2005.
(84) Tork, T.; Sadowski, G.; Arlt, W.; De Haan, A.; Krooshof, G. Modelling of High-Pressure Phase Equilibria Using the Sako-Wu-Prausnitz Equation of State: II. Vapour-Liquid Equilibria and Liquid-Liquid Equilibria in Polyolefin Systems. *Fluid Phase Equilib.* **1999**, *163* (1), 79−98.

https://doi.org/10.1021/acssuschemeng.3c05521
ACS Sustainable Chem. Eng. XXXX, XXX, XXX−XXX